PCCP

PAPER

View Article Online
View Journal | View Issue

Cite this: *Phys. Chem. Chem. Phys.*, 2017, **19**, 2583

Interactions of methanol, ethanol, and 1-propanol with polar and nonpolar species in water at cryogenic temperatures

Ryutaro Souda

Received 26th October 2016,
Accepted 21st December 2016

DOI: 10.1039/c6cp07313a

www.rsc.org/pccp

Published on 06 January 2017. Downloaded on 22/01/2017 10:16:52.

Methanol is known as a strong inhibitor of hydrate formation, but clathrate hydrates of ethanol and 1-propanol can be formed in the presence of help gases. To elucidate the hydrophilic and hydrophobic effects of alcohols, their interactions with simple solute species are investigated in glassy, liquid, and crystalline water using temperature-programmed desorption and time-of-flight secondary ion mass spectrometry. Nonpolar solute species embedded underneath amorphous solid water films are released during crystallization, but they tend to withstand water crystallization under the coexistence of methanol additives. The CO_2 additives are released after crystallization along with methanol desorption. These results suggest strongly that nonpolar species that are hydrated (*i.e.*, caged) associatively with methanol can withstand water crystallization. In contrast, ethanol and 1-propanol additives weakly affect the dehydration of nonpolar species during water crystallization, suggesting that the former tend to be caged separately from the latter. The hydrophilic *vs.* hydrophobic behavior of alcohols, which differs according to the aliphatic group length, also manifests itself in the different abilities of surface segregation of alcohols and their effects on the water crystallization kinetics.

1 Introduction

Hydration of polar and nonpolar molecules in water has attracted considerable attention because numerous important processes that occur in aqueous solutions, such as protein folding and formation of micelles and biological membranes, rely on the interactions between water and non-polar moieties of organic molecules. Gas–ice interactions are also important for cometary research. Hydrophobic hydration is such that the non-polar solute species enhances the solvent water structure, producing a more ordered water structure near the hydrophobic entity.[1] The exact nature of this structural ordering has remained unclear, but the non-polar hydration process engenders a net loss of entropy. Hydrophobic hydration is not easily accessible using liquid water because of the poor solubility of non-polar species.[2,3] Therefore, it has been explored using water-soluble solute species such as alcohols.[4–7] It is known that the increase in the entropy of a water–methanol mixture is much less than that expected from an ideal solution. This phenomenon has been explained as incomplete mixing or the formation of an ice-like water structure in the solution. To date, additional insights into hydration have been gained from experiments using amorphous solid water (ASW) interaction with simple molecules, from which much might be learned about hydration,[8–15] diffusion,[16–18] proton transfer,[19–25] host–guest interactions,[26,27] and clathrate hydrate formation[28,29] for widely diverse guest species.

ASW has been investigated as a model system for liquid and glassy water. Its physical properties are influenced strongly by the deposition temperature of water molecules and post-annealing of the film.[30,31] The ASW film formed at temperatures below 70 K is characterized by a microporous structure, as evidenced by a capacity to hold large volumes of gas molecules in pores. The molecules can be confined in the film interior if pores decay before they are released. Therefore, hydration phenomena can be investigated using gas-adsorbed ASW films upon heating. A liquid-like water is formed above the glass-transition temperature (T_g = 136 K)[32] before the formation of droplets or crystal grains at T_c = 160 K, as demonstrated using time-of-flight secondary ion mass spectrometry (TOF-SIMS).[17] The crystallization kinetics of water has been discussed based on temperature-programmed desorption (TPD) because the trapped molecules are released.[33–38] Asscher and co-workers[33] reported that N_2 molecules trapped in ASW are compressed and are caged microscopically by the hydrogen-bonded water molecules from TPD and work-function measurements. Nonpolar molecules embedded underneath the ASW film are known to desorb explosively during water crystallization.[34,36] This phenomenon has been explained in terms of dynamic percolation of the

International Center for Materials Nanoarchitectonics, National Institute for Materials Science, 1-1 Namiki, Tsukuba, Ibaraki 305-0044, Japan.
E-mail: SOUDA.Ryutaro@nims.go.jp

Published on 06 January 2017. Downloaded on 22/01/2017 10:16:52.

embedded species through connected diffusion paths created at grain boundaries (the so-called "molecular volcano" mechanism).[34] Nonpolar additives are considered to have no effects on the crystallization kinetics of water. In contrast, water-miscible polar molecules can modify the ASW bulk properties because the water activity can be reduced by the hydrogen bond formation with water.[15,17] In this respect, alcohols are known as the most popular hydrate formation inhibitors. Clathrate hydrates of ethanol and 1-propanol are stabilized in the presence of help gases,[39–44] but the stability of methanol clathrate hydrate remains an open question.[44,45] Elucidating these behaviors requires elucidation of how the hydroxyl and aliphatic moieties of alcohols interact with water and what effects they exert on the coadsorbed species. However, wide-ranging (co)adsorption data of alcohols on ASW are insufficient for a molecular-scale description of their hydrophilic and hydrophobic effects leading to the clathrate hydrate formation.

As described in this paper, interactions of methanol, ethanol, and 1-propanol additives with ASW are examined in terms of surface segregation, crystallization kinetics of water, and liberation of coadsorbed species. Specifically, the alcohol–water interaction in thin films and its effects on the water crystallization kinetics are investigated through dehydration processes of coadsorbed alcohol and nonpolar species embedded underneath the ASW film based on TPD measurements. The diffusion of embedded species through ASW films and the film morphology change are monitored using TOF-SIMS. Finally, the local caging effects of alcohols are discussed based on the liberation of coadsorbed species, such as acetone, Xe, CH_4, C_2H_6, C_2F_6, and CO_2.

2 Experiment

Experiments were performed in an ultrahigh vacuum (UHV) chamber with a base pressure of $<1 \times 10^{-10}$ Torr. The TPD spectra were recorded using a quadrupole mass spectrometer (QMS; IDP 300S; Hiden Analytical Ltd) placed in a differentially pumped housing. A retractable orifice was placed approximately 3 mm distant from the sample to detect atomic and molecular species detached from the surface. TOF-SIMS measurements were made using a primary beam of 2 keV He^+ ions generated in an electron-impact-type ion gun (IQE 12/38; Specs GmbH). The ion beam was incident to the sample surface at an angle of 70° after chopping into pulses using electrostatic deflectors. To extract low-energy secondary ions efficiently, a grounded mesh was placed approximately 4 mm in front of the sample surface, and a bias voltage (±500 V) was applied to the sample. Secondary ions ejected perpendicularly to the surface were detected using a microchannel plate after passage through a field-free TOF tube. The fluence of He^+ in TOF-SIMS measurements was restricted to be below 1×10^{12} ions cm^{-2} to minimize thin film decomposition.

A Ni(111) surface was used as a substrate. It was heated several times in UHV to approx. 1300 K by electron bombardment from behind. Contaminants were removed *via* sputter-annealing cycles. The substrate was mounted on a Cu cold finger extended from a closed-cycle helium refrigerator. The cold finger temperature was monitored close to the sample position using Au(Fe)–chromel thermocouples. It was controlled using a digital temperature controller and a cartridge heater attached to the finger. The temperature was ramped at a rate of 5 K min^{-1} for both TPD and TOF-SIMS measurements. Thin films were deposited onto the clean Ni(111) surface cooled to 20 K by backfilling the UHV chamber with gaseous samples admitted through high-precision leak valves. Liquid samples of water, methanol, ethanol, 1-propanol, and acetone were degassed using several freeze–pump–thaw cycles before use. Gaseous samples of methane, ethane, perfluoroethane, and carbon dioxide were admitted from glass bottles without further purification. The purity of the deposited molecules, as well as cleanliness of the Ni(111) substrate, was checked *in situ* based on TOF-SIMS spectra. The coverage of adspecies was determined from evolution curves of secondary ion intensities as a function of exposure. It requires gas exposures of *ca.* 2.5–3 langmuirs (1 L = 1×10^{-6} Torr s) to form monolayer films on Ni(111).

3 Results

Fig. 1 displays TPD spectra of ASW films including Xe (132 amu) and methanol (31 amu) additives. They were prepared in a different manner. As Fig. 1(a) shows, the Xe TPD peak occurs at around 160 K together with a shoulder of the water TPD spectrum when the Xe adspecies (1 L) was capped with the ASW film (20 L). These behaviors are characteristics of water crystallization. Desorption of Xe might occur *via* the molecular volcano mechanism.[34] However, if methanol (1 L) and Xe (1 L) are coadsorbed underneath the ASW film (20 L), the Xe TPD peak intensity at 160 K is depressed considerably as shown in Fig. 1(b). The shoulder of the water TPD peak remains at 160 K. Results indicate that the water crystallization kinetics itself is not influenced strongly by Xe and methanol additives, but Xe tends to withstand water crystallization and to desorb along with evaporation of crystalline ice. Consequently, the liberation of embedded Xe is not explainable simply in terms of the molecular volcano mechanism through cracks of water crystallites.

The Xe TPD spectrum in Fig. 1(a) changes to that in Fig. 1(c) and (d) when 1 L and 3 L, respectively, of methanol are adsorbed on the surface of the ASW films including Xe (1 L) at the substrate interface. The temperature at which the methanol desorption rate increases correlates with the Xe peak temperature, but the shoulder of the water TPD peak becomes obscure. We assign T_c of water as the peak temperature of Xe. The methanol is released gradually after water crystallization, but the low-temperature tails exist in all methanol TPD spectra before crystallization occurs. They are ascribable to physisorbed species, as inferred from the fact that a methanol multilayer film starts to evaporate from the Ni(111) surface at around 120 K. It should be noticed that water crystallizes immediately after the glass–liquid transition at 136 K when a methanol monolayer (~3 L) is present. Consequently, methanol on the free surface reduces T_c of water more significantly than that in the film interior.

 This journal is © the Owner Societies 2017

Published on 06 January 2017. Downloaded on 22/01/2017 10:16:52.

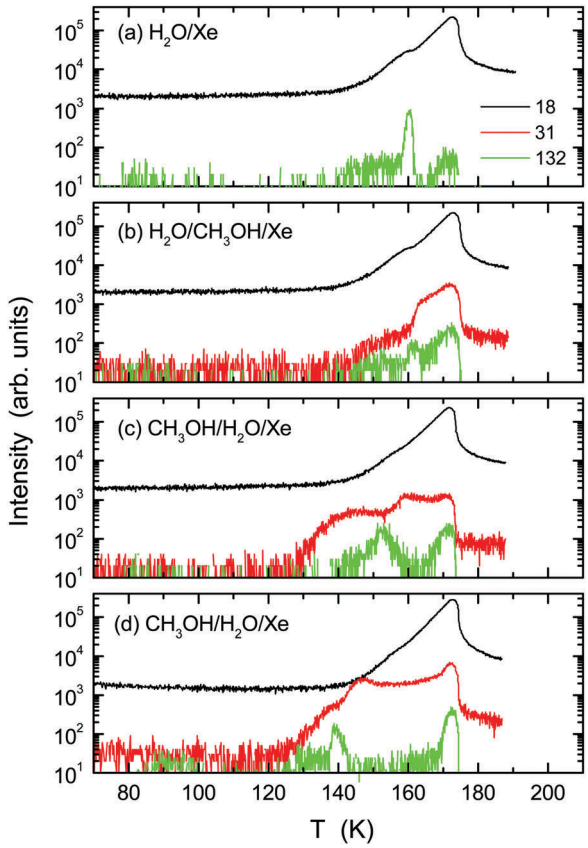

Fig. 1 TPD spectra of water (18 amu), methanol (31 amu), and Xe (132 amu) from differently tailored ASW films. (a) Xe (1 L) was capped with water (20 L). (b) Xe and methanol (1 L each) were capped with water (20 L). Xe (1 L) was capped with water (20 L) and then (c) 1 L and (d) 3 L of methanol were adsorbed on the film surface. The molecules were deposited on the Ni(111) substrate at 20 K. The temperature ramp rate was 5 K min^{-1}.

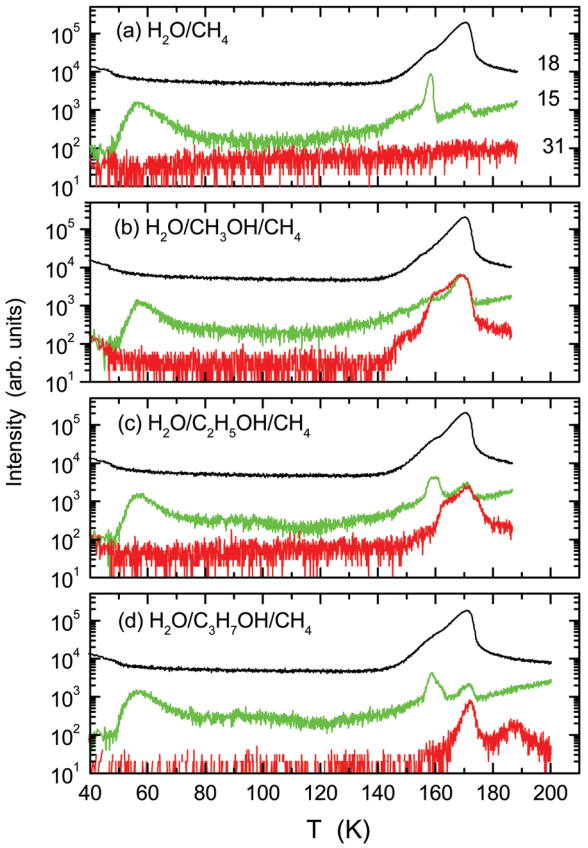

Fig. 2 TPD spectra of water (18 amu), methane (15 amu), and alcohols (31 amu) from differently tailored ASW films. (a) Methane (1 L) was deposited on Ni(111) and then it was capped with water (20 L). (b) Methane and methanol (1 L each) were capped with water (20 L). Methane (1 L) was adsorbed together with (c) ethanol or (d) 1-propanol (1 L each) on Ni(111) and then water (20 L) was deposited on them.

Fig. 2(a) displays the TPD spectrum of methane (15 amu; 1 L) deposited at the substrate interface of the ASW film (20 L). The sharp peak of methane at 160 K results from water crystallization, whereas a broad peak at around 60 K arises from physisorbed methane. The shape of the former is fundamentally the same as that obtained using Xe, as presented in Fig. 1(a), although the latter is almost absent for Xe. The multilayers of Xe and methane desorb from Ni(111) at around 60 and 40 K, respectively (not shown). Therefore, it might be presumed that pores collapse at *ca.* 50–60 K to explain the higher trapping rate of Xe than methane. In reality, however, ASW pores are known to remain up to *ca.* 120 K.[31] Actually, Xe is likely to be entrapped at specific sites (probably higher coordinate sites) of porous ASW films more preferentially than methane. This behavior might also be associated with the fact that Xe forms a stable clathrate when heated from a solid solution of Xe and ASW.[27]

Effects of alcohols on methane desorption are examined by coadsorption of methanol, ethanol, and 1-propanol additives (2 L each) with methane (1 L) at the substrate interface of the ASW film (20 L). As shown in Fig. 2(b), the methane peak at 160 K is depressed by the coexistence of methanol. The characteristic shoulder of the water TPD peak at 160 K becomes weaker. The entrapped methane is released along with the evaporation of water and methanol at around 170 K. The result is fundamentally identical to that for Xe (Fig. 1(b)). In contrast, the methane liberation at 160 K is not significantly reduced under the coexistence of ethanol or 1-propanol, as shown in Fig. 2(c) and (d). No alcohols have any appreciable effect on the desorption of physisorbed methane at 60 K.

Fig. 3 displays temperature-programmed TOF-SIMS intensities for the ASW films (20 L) including (a) methanol, (b) ethanol, and (c) 1-propanol additives (2 L each) at the substrate interface. In the case of methanol, the CH_3^+ intensity tends to increase at temperatures higher than 140 K and the H^+ and H_3O^+ intensities decrease at 150 K because of methanol segregation to the surface. At this temperature, the Ni^+ ion starts to evolve as a result of ASW film dewetting. The pure ASW film dewets the Ni(111) substrate during crystallization at T_c = 160 K. Therefore, T_c can be reduced by the surface segregated methanol species. This behavior is consistent with the TPD measurements shown in Fig. 1(c) and (d), where the Xe peak shifts to lower temperatures when methanol exists on the ASW film surface. The shoulder in the water TPD spectrum in Fig. 2(b) is shifted and weakened, which occurs in association with the gradual film morphology

Published on 06 January 2017. Downloaded on 22/01/2017 10:16:52.

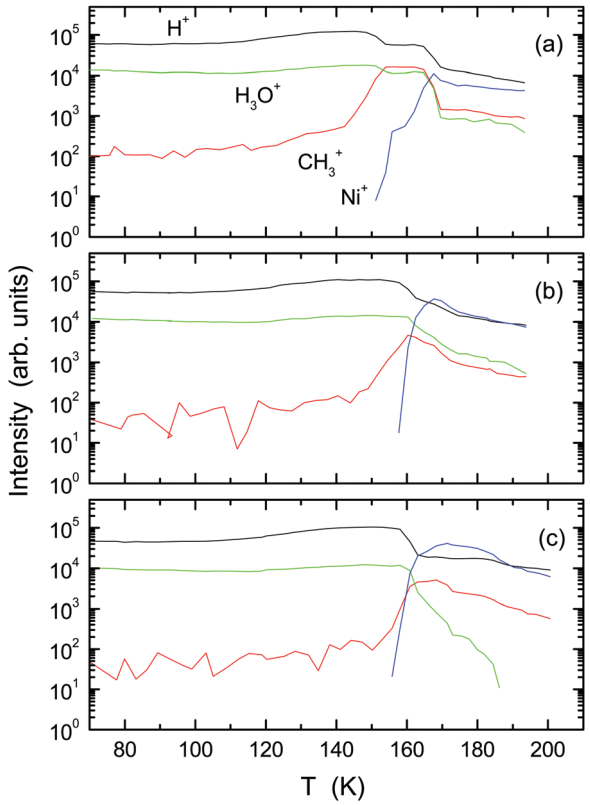

Fig. 3 Temperature-programmed TOF-SIMS intensities of H^+, H_3O^+, CH_3^+ and Ni^+ ions from ASW films (20 L) including (a) methanol, (b) ethanol, and (c) 1-propanol (2 L each) at the interface with Ni(111).

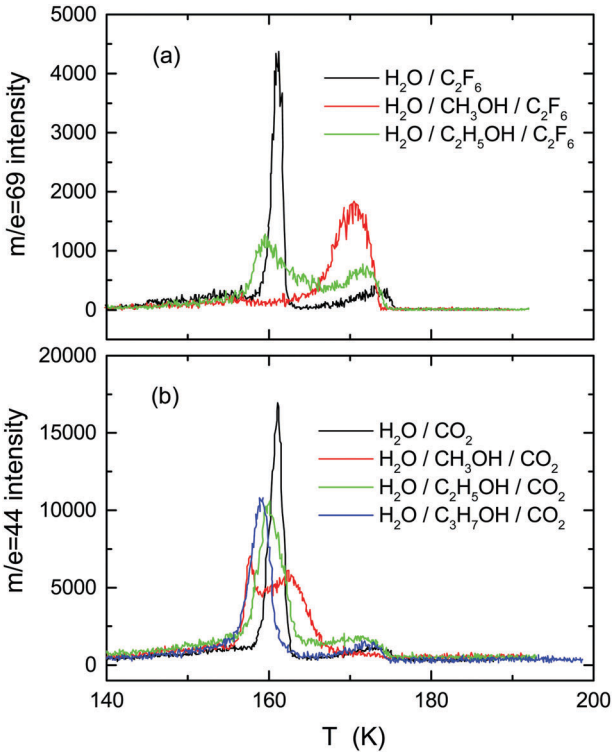

Fig. 4 TPD spectra of (a) C_2F_6 and (b) CO_2 (1 L each) deposited with and without alcohols (2 L each) at the substrate interface of the ASW films (20 L).

change occurring at 150–170 K, as depicted in Fig. 3(a). In contrast to methanol, the ethanol and 1-propanol adspecies tend to remain in the ASW film interior until crystallization occurs at 160 K, as revealed from the evolution curves of TOF-SIMS intensities in Fig. 3(b) and (c). Consequently, dewetting of ASW is associated with water crystallization; T_c is reduced preferentially by methanol additives.

Fig. 4 displays TPD spectra of (a) C_2F_6 and (b) CO_2 adspecies (1 L each) with and without coadsorbed alcohols (2 L) at the substrate interface of the ASW films (20 L). The spectral shapes shown for C_2F_6 and CO_2 without alcohols are almost identical. The coadsorbed methanol changes the C_2F_6 peak shape to a greater degree than ethanol does. The peak at 160 K almost disappears by methanol, but it persists under the coexistence of ethanol. The C_2F_6 molecules that withstood water crystallization are released during evaporation of water at *ca.* 170 K. These results are fundamentally identical to those using Xe and methane adspecies. In contrast, the effects of alcohols on CO_2 desorption are weak. A unique feature is observed when methanol coexists: A sharp peak of CO_2 at 157 K is a characteristic of water crystallization, which is followed by a broad peak at 163 K instead of the common 170 K peak resulting from evaporation of the crystalline ice. An interesting fact is that the peak temperature corresponds well to the desorption onset of methanol. Here, the methanol TPD spectrum is not shown but it is identical to that in Fig. 1(b) and 2(b). The fact that CO_2 is liberated together with methanol implies that their associative interaction plays an important role. In contrast, ethanol and 1-propanol additives have weaker effects on CO_2 desorption during and after water crystallization.

Given the context presented above, how alcohols interact with CO_2 across the ASW films demands further explanation. Fig. 5 represents TPD spectra of ASW films (20 L) prepared by deposition of CO_2 (1 L) at the substrate interface and adsorption of (a) methanol, (b) ethanol, and (c) 1-propanol (2 L each) on the film surface. As described already, the methanol adspecies on the film surface reduces T_c of water, so that CO_2 desorbs at *ca.* 140 K. The physisorbed methanol starts to desorb from the film surface at temperatures higher than 120 K. Then the desorption rate of methanol increases after water crystallization at *ca.* 145–150 K. Therefore, no strong correlation is identified in the desorption of methanol and CO_2 in this case because they tend to interact independently with water. The reduction of T_c by methanol is fundamentally identical to that probed using Xe (Fig. 1(c) and (d)). The ethanol adspecies reduces T_c of water to some extent, but the effect of 1-propanol adspecies is insignificant.

Fig. 6(a) displays TPD spectra obtained for coadsorption of acetone (2 L) and ethane (1 L) at the substrate interface of the ASW film (20 L). The TPD spectra of acetone (43 amu) and ethane (26 amu) form peaks at T_c = 160 K. The ethane TPD spectrum without acetone is almost identical to that in Fig. 6(a) (not shown). The TPD spectrum of acetone resembles that of nonpolar species except that the high-temperature tail of the 160 K peak is conspicuous until the leading edge of the water TPD peak. Fig. 6(b) shows that T_c of water is unchanged when

 This journal is © the Owner Societies 2017

Published on 06 January 2017. Downloaded on 22/01/2017 10:16:52.

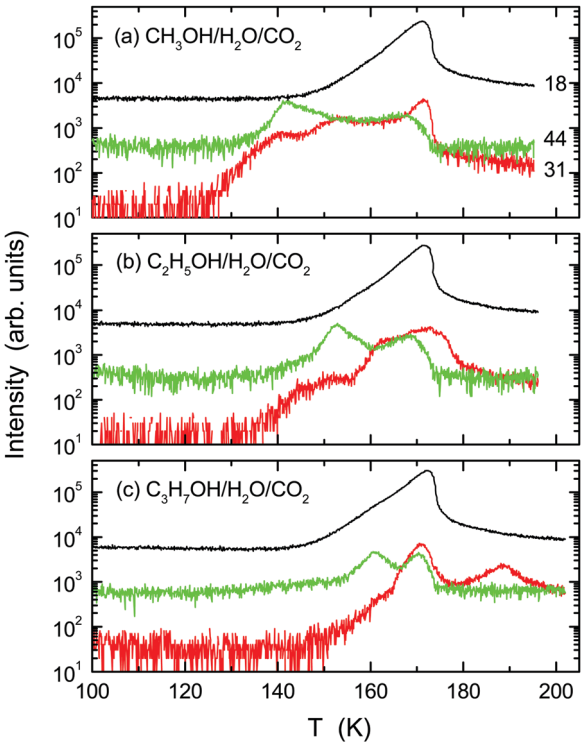

Fig. 5 TPD spectra of water (18 amu), CO_2 (15 amu), and alcohols (31 amu) from ASW films (20 L) that include CO_2 (1 L) at the substrate interface and (a) methanol, (b) ethanol, and (c) 1-propanol (2 L each) adsorbed on the film surface.

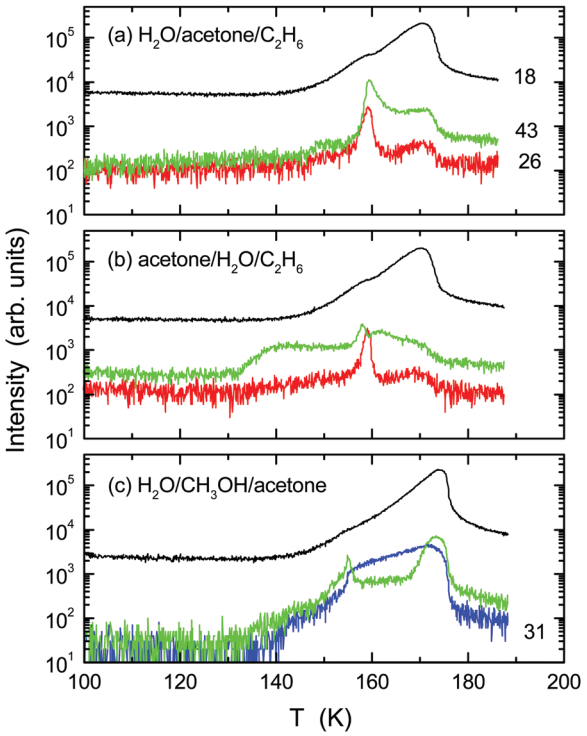

Fig. 6 TPD spectra of water (18 amu), ethane (26 amu), and acetone (43 amu) from ASW films (20 L) including (a) ethane and acetone (1 L each) at the substrate interface and (b) ethane at the substrate interface and acetone on the film surface. (c) TPD spectra of water, acetone, and methanol (31 amu) from ASW films (20 L) including acetone (1 L) and methanol (2 L) at the substrate interface.

acetone (2 L) is adsorbed on the ASW film surface, as evidenced by the occurrence of the ethane peak and the water shoulder at 160 K. The acetone TPD peak is broadened considerably because the hydrogen-bonded acetone desorbs gradually, resulting in a relatively small acetone peak at *ca.* 160 K. The experimental result for coadsorption of acetone (1 L) and methanol (2 L) at the substrate interface of the ASW film is displayed in Fig. 6(c). The acetone peak during water crystallization is weakened and shifted to 155 K under the coexistence of methanol. Most of the acetone is liberated during evaporation of the crystalline ice at 170 K. Consequently, acetone behaves similarly to a nonpolar species in interaction not only with water but also with coadsorbed methanol.

4 Discussion

The ASW film dewets the Ni(111) substrate during crystallization with and without alcohol additives deposited at the substrate interface as shown in Fig. 3. In the framework of the molecular volcano, the nonpolar species at the substrate interface of ASW must be released during film dewetting (*i.e.*, crystallization), but this release does not hold when methanol coexists. Apparently, the interaction between water and additives is not elucidated simply in terms of the molecular volcano mechanism. Upon heating, the nonpolar additives are incorporated into the interior of the porous ASW film, caged by water molecules (*i.e.* hydrated), and liberated *via* disintegration of the cage. In contrast, alcohols are hydrated such that their hydroxyl groups enter the hydrogen bond network of water. The network structure of water is broken or modified significantly by hydrated alcohols because one hydrogen bond is replaced by the aliphatic group, leading to rearrangement of the water molecules to form a cage around the aliphatic moiety. The formation of such a modified cage is expected to have a significant effect on hydration and dehydration of coadsorbed species. The occurrence of this effect is especially true for methanol. However, cages of hydrated ethanol and 1-propanol appear to have a relatively weak effect, as evidenced by the occurrence of the dehydration peak of the nonpolar species during water crystallization, as shown in Fig. 2 and 4. Acetone has no appreciable effect on the water crystallization kinetics and dehydration of coadsorbed ethylene, indicating that the polar carbonyl group of acetone does not modify the hydrogen-bond network or the cage structure of water in contrast to the hydroxyl group of alcohols.

Dehydration of nonpolar species, or cage collapse, is thought to occur during the first-order phase transition of water. In general, a liquid-like phase is expected to be formed prior to crystallization, but the assignment of water's T_g has persisted as a controversial subject in calorimetric studies. Johari *et al.*[32] observed an unusually small endotherm at 136 K and assigned it as water's T_g. However, T_g has been reassigned to 165 ± 5 K in comparison with calorimetric data of other inorganic glasses.[46] Based on self-diffusion measurements using TOF-SIMS, we have

Published on 06 January 2017. Downloaded on 22/01/2017 10:16:52.

observed that a liquid-like water evolves at temperatures higher than T_g = 136 K.[17] In the framework of polyamorphism,[47] the liquid formed at this temperature is a distinct phase designated as low density liquid (LDL). The local hydrogen-bond structure of LDL resembles that of ASW and crystalline ice rather than that of normal liquid water.[48] Therefore, if LDL transformed directly into the crystalline ice Ic, the cage would be retained without dehydration of the nonpolar species. This behavior is elucidated if the first order liquid–liquid (L–L) phase transition occurs prior to crystallization:[37] LDL transforms into supercooled (*i.e.*, normal) water and then it crystallizes immediately into ice Ic. Therefore, dehydration might be a characteristic of the L–L transition rather than crystallization of water.

The nonpolar molecules are trapped in the film interior during pore collapse, so that an ice-like cage is likely to be formed locally in ASW and LDL at cryogenic temperatures. In this respect, results of earlier studies of clathrate hydrates might be instructive. Small atomic and molecular species form structure I and structure II type clathrate hydrates through occupation of small and large cages.[43,44] Small alcohols are known to be inhibitors for clathrate hydrate formation. However, ethanol and 1-propanol offer less hydrate inhibition than methanol for comparable aqueous molar concentrations.[43] In fact, several stable and metastable hydrates have been reported for ethanol and 1-propanol including the formation of the structure II clathrate hydrate at cryogenic temperatures.[39–42] On the other hand, transmission electron microscopy and electron diffraction studies of water–methanol mixtures have also suggested that the structure-II clathrate hydrate of methanol is formed after water crystallization.[28] Consequently, it is considered that clathrate-like structures might be formed for all alcohols studied here. In line with this conjecture, the fact that the ethanol and 1-propanol additives tend to stay in the ASW film interior until dewetting occurs (Fig. 3) might be explained as cage formation in water. In contrast, the surface segregation of methanol suggests strongly that the methyl moiety is not caged sufficiently in the film interior. Moreover, it is noteworthy that the methanol adspecies on the ASW film surface reduces water's T_c (Fig. 5) considerably, indicating that the nucleation is initiated at the free surface in the presence of methanol. This nucleation occurs because the surface free energy is reduced by methanol *via* termination of the free hydroxyl group of water. The enhanced mobility of the molecules on the free surface also facilitates microscopic structural rearrangements for crystallization. The relatively weak effects by the ethanol and 1-propanol additives on water crystallization kinetics imply that the clathrate-like cage tends to be formed in the near surface region as well. These results are consistent with those obtained from MD simulations:[44] the ethanol and 1-propanol guests induce distortion of the cage faces because of high hydrogen-bonding probability (>50%). However, the hydrate lattice itself tends to decompose for the methanol guest at higher temperatures. Regarding the interactions between nonpolar species and alcohols in ice, ethanol and 1-propanol are known to act as promoters to form binary structure-II clathrate hydrates in the presence of small help gas molecules such as CH_4 and CO_2.[43] For stabilization of the structure-II clathrate hydrates, sufficiently large aliphatic alcohols are necessary to fill the larger cage, together with filling of the smaller cage with nonpolar species.[44] Although no direct evidence points to formation of gas hydrates of methanol, methanol might also be incorporated into the hydrate lattice along with other guest molecules.[45] Consequently, methanol can accelerate the capture of nonpolar species into crystalline water in comparison with the ethanol and 1-propanol additives, but this phenomenon appears to have nothing to do with the formation of binary clathrate hydrates.

Although ordered clathrate hydrates are not formed, it is likely that clathrate-like cages are created in a disorderly fashion around nonpolar species and alcohols in ASW and LDL because their local structure resembles that of crystalline ice. To date, several experimental techniques have been used to examine the local structures of amorphous solid mixtures formed by vapor deposition. Mayer and Hallbrucker[49,50] and Nakayama *et al.*[51] reported that a cage-like structure is maintained locally even in the amorphous phase. Yamamuro and co-workers[27] demonstrated that hydrogen bonds strengthen with increasing van der Waals diameter of solutes and that the Xe atom is the most suitable for hydrophobic hydration among guest species such as Ar, CD_4, Xe, and SF_6. Using FT-IR, Fleyfel and Devlin[29] reported that structure-I and structure-II clathrate hydrates of CO_2 can be grown epitaxially to the substrates of ethylene-oxide and tetrahydrofuran clathrate hydrates at $T < 160$ K. Results of the present study show that the TPD peaks of Xe, CH_4, and CO_2 have almost identical shape without alcohol additives because they interact weakly with local cage walls of pure water molecules. That Xe is hydrated more preferentially than CH_4 (see Fig. 1 and 2) is consistent with the fact that Xe forms a stable clathrate.[27] However, the clathrate-like cages of all nonpolar species examined for the present study are disintegrated during the water phase transition unless alcohol additives coexist.

The structure and stability of the local cage are expected to be changed by the coexistence of alcohol additives, so that the hydration and dehydration processes of nonpolar species during and after water crystallization can be modified. If the alcohol and nonpolar species are caged independently by water, the dehydration process is expected to be influenced weakly by alcohols. Probably, such is the case for the ethanol and 1-propanol additives in ASW and LDL, as inferred from the possible structure of the binary clathrate hydrates.[44] The apparently different behavior of methanol in ASW implies that the methyl moiety is so small that it cannot be caged sufficiently in water. However, a cage might be formed if methanol is consolidated with nonpolar species. The stability of such a cage is expected to differ from that of the pure-water cage against the L–L phase transition because the water–methanol hydrogen bonds play a role. In this respect, it must be noted that the CO_2 molecules desorb together with methanol after crystallization (see Fig. 4), suggesting that CO_2 is caged in direct contact with methanol to withstand water crystallization. After crystallization, the complex does not necessarily evolve into binary clathrate hydrates because the solute species can be trapped solely at grain boundaries. The grain-boundary phase, which exhibits a liquid like property,[52]

 This journal is © the Owner Societies 2017

might be responsible for specificity of the dehydration processes after crystallization. The complex decays to desorb CO_2, whereas the Xe, CH_4, C_2H_6, and C_2F_6 species can be trapped independently with methanol, leading to their desorption along with the evaporation of water crystal grains. Consequently, caged species with and without alcohols are thought to be formed by codeposition of nonpolar species at cryogenic temperatures; they can be arranged randomly in glassy, liquid, and crystalline water without forming ordered clathrate hydrates.

5 Conclusion

Interactions of methanol, ethanol and 1-propanol with water were examined through their effects on water crystallization kinetics and dehydration of coadsorbed species such as acetone, Xe, CH_4, C_2H_6, C_2F_6, and CO_2. The hydrogen bond network of water is modified considerably by inclusion of methanol's hydroxyl group, as evidenced by the fact that the monolayer of methanol on the free surface of ASW reduces T_c to 140 K from the pure water value of 160 K. The T_c modification effect of alcohols is weakened with increasing size of the aliphatic group. The methanol additives embedded underneath the ASW film segregate to the free surface whereas the ethanol and 1-propanol additives tend to stay in the ASW film interior. These behaviors are thought to be related to the caging ability of the aliphatic moieties in the ASW film interior and near surface region, as inferred from the clathrate hydrate formation for alcohols. The methanol is not caged sufficiently in water; it tends to segregate to the surface to terminate the free OH group. The nonpolar molecules embedded underneath the ASW film are released during the water phase transition, but they can withstand film dewetting during crystallization under the coexistence of methanol. This behavior is not explicable by the simple molecular volcano picture. The nonpolar species might be stabilized to form a microscopic cage together with methanol to survive the L–L phase transition. Consequently, methanol can accelerate the capture of nonpolar species into the crystalline ice. In contrast, a smaller amount of nonpolar species withstands water crystallization under the coexistence of ethanol and 1-propanol, suggesting that the nonpolar species and the alcohols tend to be caged separately in water.

References

1 H. S. Frank and M. W. Evans, *J. Chem. Phys.*, 1945, **135**, 507.
2 P. Buchanan, N. Aldiwan, A. K. Soper, J. L. Creek and C. A. Koh, *Chem. Phys. Lett.*, 2005, **415**, 89.
3 C. A. Koh, R. P. Wisbey, X. Wu and R. E. Westacott, *J. Chem. Phys.*, 2000, **113**, 6390.
4 A. K. Soper and J. L. Finney, *Phys. Rev. Lett.*, 1993, **71**, 4346.
5 D. T. Bowron, A. K. Soper and J. L. Finney, *J. Chem. Phys.*, 2001, **114**, 6203.
6 S. Dixit, J. Crain, W. C. K. Poon, J. L. Finney and A. K. Soper, *Nature*, 2002, **416**, 829.
7 J. H. Guo, Y. Luo, A. Augustsson, S. Kashtanov, J. E. Rubensson and D. K. Shuh, *Phys. Rev. Lett.*, 2003, **91**, 157401.
8 H. Ogasawara, N. Horimoto and M. Kawai, *J. Chem. Phys.*, 2000, **112**, 8229.
9 J. Günster, G. Liu, J. Stultz and D. W. Goodman, *J. Chem. Phys.*, 1999, **110**, 2558.
10 S. Krischok, O. Höfft, J. Günster, J. Stultz, D. W. Goodman and V. Kempter, *Surf. Sci.*, 2001, **495**, 8.
11 J. Günster, G. Liu, J. Stultz, S. Krischok and D. W. Goodman, *J. Phys. Chem. B*, 2000, **104**, 5738.
12 S. Bahr and V. Kempter, *J. Chem. Phys.*, 2009, **130**, 214509.
13 R. G. Bhuin, R. R. J. Methikkalam, B. Sivaraman and T. Pradeep, *J. Phys. Chem. C*, 2015, **119**, 11524.
14 R. Souda, *J. Phys. Chem.*, 2016, **120**, 934.
15 R. Souda, *Chem. Phys. Lett.*, 2016, **645**, 27.
16 R. C. Bell, H. Wang, M. J. Iedama and J. P. Cowin, *J. Am. Chem. Soc.*, 2003, **125**, 5176.
17 R. Souda, *Phys. Rev. Lett.*, 2004, **93**, 235502.
18 J. Cyriac and T. Pradeep, *J. Phys. Chem. C*, 2007, **111**, 8557.
19 S. C. Park, K. H. Jung and H. Kang, *J. Chem. Phys.*, 2004, **121**, 2765.
20 S. C. Park and H. Kang, *J. Phys. Chem. B*, 2005, **109**, 5124.
21 S. C. Park, K. W. Maeng, T. Predeep and H. Kang, *Angew. Chem., Int. Ed.*, 2001, **40**, 1497.
22 S. C. Park, T. Pradeep and H. Kang, *J. Chem. Phys.*, 2000, **113**, 9373.
23 J. Cyriac and T. Pradeep, *J. Phys. Chem. C*, 2008, **112**, 5129.
24 R. Souda, *J. Chem. Phys.*, 2003, **119**, 6194.
25 M. Kondo, H. Kawanowa, Y. Gotoh and R. Souda, *J. Chem. Phys.*, 2004, **121**, 8589.
26 O. Yamamuro, Y. Madokoro, H. Yamasaki, T. Matsuo, I. Tsukushi and K. Takeda, *J. Chem. Phys.*, 2001, **115**, 9808.
27 T. Kikuchi, Y. Inaura, N. Onda-Yamamuro and O. Yamamuro, *J. Phys. Soc. Jpn.*, 2012, **81**, 094604.
28 D. Blake, L. Allamandola, S. Sandford, D. Hudgins and F. Freund, *Science*, 1991, **254**, 548.
29 F. Fleyfel and J. P. Devlin, *J. Phys. Chem.*, 1991, **95**, 3811.
30 K. P. Stevenson, G. A. Kimmel, Z. Dohnalek, R. S. Smith and B. D. Kay, *Science*, 1999, **283**, 1505.
31 G. A. Kimmel, K. P. Stevenson, Z. Dohnalek, R. S. Smith and B. D. Kay, *J. Chem. Phys.*, 2001, **114**, 5284.
32 G. P. Johari, A. Hallbrucker and E. Mayer, *Nature*, 1987, **330**, 552.
33 T. Livneh, L. Romm and M. Asschar, *Surf. Sci.*, 1996, **351**, 250.
34 R. S. Smith, C. Huang, E. K. L. Wong and B. D. Kay, *Phys. Rev. Lett.*, 1997, **79**, 909.
35 Y. Lilach and M. Asscher, *J. Chem. Phys.*, 2002, **117**, 6730.
36 M. P. Collings, M. A. Anderson, R. Chen, J. W. Dever, S. Viti, D. A. Williams and M. R. S. McCoustra, *Mon. Not. R. Astron. Soc.*, 2004, **354**, 1133.
37 R. Souda, *J. Chem. Phys.*, 2006, **125**, 181103.
38 R. A. May, R. S. Smith and B. D. Kay, *Phys. Chem. Chem. Phys.*, 2011, **13**, 19848.
39 A. D. Potts and D. W. Davidson, *J. Phys. Chem.*, 1965, **69**, 996.
40 P. Boutron and A. Kaufmann, *J. Chem. Phys.*, 1978, **68**, 5032.
41 J. B. Ott, J. R. Goates and B. A. Waite, *J. Chem. Thermodyn.*, 1979, **11**, 739.

Published on 06 January 2017. Downloaded on 22/01/2017 10:16:52.

42 Y. M. Zelenin, *J. Struct. Chem.*, 2003, **44**, 130.
43 A. Anderson, A. Chapoy, H. Haghighi and B. Tohidi, *J. Phys. Chem. C*, 2009, **113**, 12602.
44 S. Alavi, S. Takeya, R. Ohmura, T. K. Woo and J. A. Ripmeester, *J. Chem. Phys.*, 2010, **133**, 074505.
45 K. Shin, K. A. Udachin, I. L. Moudrakovski, D. M. Leek, S. Alavi, C. I. Ratcliffe and J. A. Ripmeester, *Proc. Natl. Acad. Sci. U. S. A.*, 2013, **110**, 8437.
46 V. Velikov, S. Borick and C. A. Angell, *Science*, 2011, **294**, 2335.
47 O. Mishima and H. E. Stanley, *Nature*, 1998, **396**, 329.
48 J. L. Finney, A. Hallbrucker, I. Kohl, A. K. Soper and D. T. Bowron, *Phys. Rev. Lett.*, 2002, **88**, 225503.
49 E. Mayer and A. Hallbrucker, *J. Chem. Soc., Chem. Commun.*, 1989, **12**, 749.
50 A. Hallbrucker and E. Mayer, *J. Chem. Soc., Faraday Trans.*, 1990, **86**, 3785.
51 H. Nakayama, D. D. Krug, C. L. Ratcliff and J. A. Ripmeester, *Chem. – Eur. J.*, 2003, **9**, 2969.
52 R. Souda, *Phys. Chem. Chem. Phys.*, 2014, **16**, 1095.

Published on 06 January 2017. Downloaded on 22/01/2017 10:16:52.

This journal is © the Owner Societies 2017